CHEMISTRY

Favoring the unfavored: Selective electrochemical nitrogen fixation using a reticular chemistry approach

Hiang Kwee Lee,[1,2] Charlynn Sher Lin Koh,[1] Yih Hong Lee,[1] Chong Liu,[1]* In Yee Phang,[2] Xuemei Han,[1] Chia-Kuang Tsung,[3] Xing Yi Ling[1†]

Copyright © 2018 The Authors, some rights reserved; exclusive licensee American Association for the Advancement of Science. No claim to original U.S. Government Works. Distributed under a Creative Commons Attribution NonCommercial License 4.0 (CC BY-NC).

Electrochemical nitrogen-to-ammonia fixation is emerging as a sustainable strategy to tackle the hydrogen- and energy-intensive operations by Haber-Bosch process for ammonia production. However, current electrochemical nitrogen reduction reaction (NRR) progress is impeded by overwhelming competition from the hydrogen evolution reaction (HER) across all traditional NRR catalysts and the requirement for elevated temperature/pressure. We achieve both excellent NRR selectivity (~90%) and a significant boost to Faradic efficiency by 10 percentage points even at ambient operations by coating a superhydrophobic metal-organic framework (MOF) layer over the NRR electrocatalyst. Our reticular chemistry approach exploits MOF's water-repelling and molecular-concentrating effects to overcome HER-imposed bottlenecks, uncovering the unprecedented electrochemical features of NRR critical for future theoretical studies. By favoring the originally unfavored NRR, we envisage our electrocatalytic design as a starting point for high-performance nitrogen-to-ammonia electroconversion directly from water vapor–abundant air to address increasing global demand of ammonia in (bio) chemical and energy industries.

INTRODUCTION

Fixation of naturally abundant nitrogen (N_2) into ammonia is a key (bio)chemical transformation required to sustain life (*1*–*3*), with ammonia heavily used as fertilizers, feedstock to numerous chemical and pharmaceutical productions, and also potential carbon-free condensed fuel. Among various (bio)chemical strategies to fix N_2 (*4*–*8*), electrochemical N_2 reduction reaction (NRR) to produce ammonia is particularly promising due to its facile integration with electrochemical cells powered by renewable energy (*9*, *10*) and its versatility in using water/organic additives as alternative hydrogen (H)-atom source for NRR. NRR is further able to address the unsustainable and energy-intensive Haber-Bosch process for ammonia generation, which requires harsh operating conditions (>150 bar; >450°C) and hydrogen gas reformed from fossil fuel as a precursor (*4*, *11*). However, current progress in electrochemical NRR is inhibited by the intense competition from the hydrogen evolution reaction (HER) of water due to the preferential adsorption of H atom over nitrogen (N) atom on virtually all traditional NRR metal catalysts (including Fe, Rh, and Ru) (*3*, *12*, *13*). HER also creates overwhelming electrochemical current interference even at trace water levels (such as the omnipresence of atmospheric water vapor), thus prohibiting the direct identification of intrinsic NRR electrochemical features which are critical for future thermodynamic and kinetic studies/validations (*12*, *13*). Consequently, a majority of NRR studies report low Faradic efficiency of ≤1% even at elevated temperature/pressure (*14*, *15*). Although notable Faradic efficiency of ~35% for NRR has been recently achieved using N_2 and steam in a molten hydroxide suspension (*9*), this method requires an additional input of energy to sustain the mandatory high-temperature (200°C) and high-pressure (>25 bar) conditions. To progress toward achieving both selective and high-performance NRR at ideal ambient operations, we will need to devise new electrocatalytic design to effectively suppress water electrolysis while simultaneously promoting solid catalyst-gas interactions (*16*, *17*).

Here, we achieve both efficient and selective NRR at ambient conditions by introducing a hydrophobic layer of zeolitic imidazolate framework-71 (ZIF) over the NRR electrocatalyst's surfaces to suppress competing HER and enhance reactant-catalyst interactions. Our reticular chemistry approach focuses on exploiting ZIF's superhydrophobicity to inhibit the access of water molecules to the encapsulated electrocatalytically active surfaces (thereby inhibiting HER) and uses the high gas sorptivity of the metal-organic framework (MOF) to concentrate N_2 directly at the catalyst surface (*18*–*22*). Extensive cyclic voltammetric investigations unravel unprecedented electrochemical responses directly attributed to NRR. By quantifying the ammonia generated, we show that ZIF encapsulation enables excellent selectivity toward NRR (~90%) and significantly boosts the Faradic efficiency by ten percentage points. Finally, we demonstrate that the molecular enrichment effect imparted by ZIF can continuously facilitate and sustain NRR in such catalyst@MOF hybrid simply under prolonged N_2 bubbling. Our electrocatalytic design can also be easily extended to other materials, thereby establishing a versatile "build-on" strategy to significantly improve the electrochemical performance of a water-sensitive reaction. Our findings also offer valuable insights to expedite progress toward efficient nitrogen-to-ammonia electroconversion directly from atmospheric air where water vapor is prevalent.

RESULTS

Fabrication and characterization of ZIF-coated Ag-Au platform (Ag-Au@ZIF)

Our model NRR electrocatalyst is a bimetallic design prepared by depositing Ag nanocubes (HCl-treated; edge length, 119 ± 4 nm; fig. S1) onto an Au electrode, where the Ag-Au platform also serves as a surface-enhanced Raman scattering (SERS) platform to monitor molecular environment near the electrocatalytically active surface (*23*). We subsequently coat the electrocatalyst with a bifunctional ZIF thin film (Fig. 1A), which acts as a sorption layer to confine electroactive species

[1]Division of Chemistry and Biological Chemistry, School of Physical and Mathematical Sciences, Nanyang Technological University, 21 Nanyang Link, Singapore 637371, Singapore. [2]Institute of Materials Research and Engineering, Agency for Science, Technology and Research (A*STAR) #08-03, 2 Fusionopolis Way, Innovis, Singapore 138634, Singapore. [3]Department of Chemistry, Merkert Chemistry Center, Boston College, Chestnut Hill, MA 02467, USA.
*Present address: Department of Chemistry and Biochemistry, University of California, Los Angeles, Los Angeles, CA 90095, USA.
†Corresponding author. Email: xyling@ntu.edu.sg

Downloaded from http://advances.sciencemag.org/ on August 19, 2018

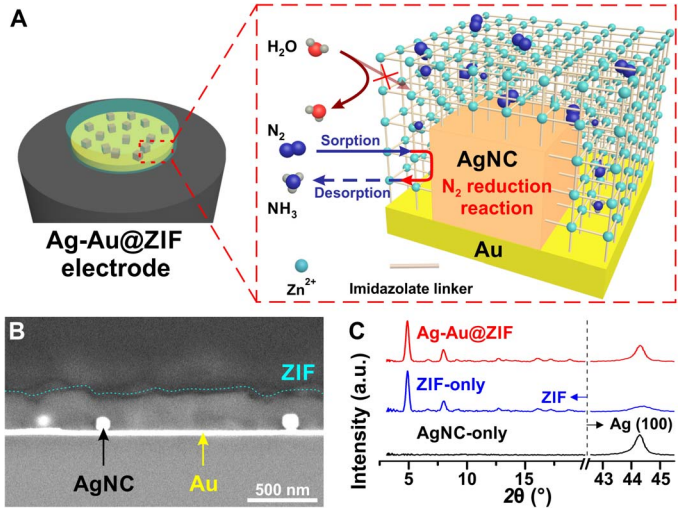

Fig. 1. Characterization of as-synthesized ZIF thin film fabricated over Ag nanocube array on Au working electrode (Ag-Au@ZIF). (**A**) Schematic depicting the importance of Ag-Au@ZIF as water repellent and nitrogen (N_2) molecular concentrator for subsequent application in electrochemical NRR into ammonia (inset). HCl-treated Ag nanocube is denoted as AgNC. (**B**) Cross-sectional scanning electron microscopy (SEM) image of Ag-Au@ZIF using an 18-nm Au film as proxy. (**C**) Substrate XRD diffraction pattern of HCl-treated AgNC, neat ZIF thin film, and as-synthesized Ag-Au@ZIF (bottom to top). a.u., arbitrary units.

near catalyst, as well as a superhydrophobic barrier to inhibit the access of water (*19*, *20*, *24*, *25*). In a typical fabrication, we use a wet chemical deposition approach to deposit ZIF on the Ag-Au platform (Ag-Au@ZIF). The synthetic process begins with an initial nucleation of ZIF on both the Au and Ag surfaces, followed by its overgrowth into an extended polycrystalline thin film (thickness, 321 ± 17 nm; Fig. 1B and fig. S2, A to C). Ag-Au@ZIF exhibits unique x-ray diffraction (XRD) patterns equivalent to those in neat ZIF thin film and Ag nanocubes (Fig. 1C and fig. S2D) (*26*), denoting the formation of a pristine MOF membrane over the Ag-Au electrode.

Our Ag-Au@ZIF design uses ZIF as a hydrophobic barrier for N_2 to selectively access the enclosed electrocatalyst while concurrently blocking the entry of water (*24*, *25*). Note that electrochemical reactions are mainly confined to the enclosed Ag-Au metal surfaces in our setup rather than the MOF coating, which is directly exposed to the electrolyte because ZIF is a poor electrical conductor (fig. S2E) (*27*). The overgrowth of ZIF on metallic nanoparticles using our fabrication protocol generates nanoscopic interfacial cavities at the interface between the catalyst surface and the polycrystalline ZIF coating (fig. S2, F to H) (*18*). Collectively, these interfacial cavities and MOF's intrinsic micropores are essential for accumulating N_2 and other reactant molecules at the catalytic surface for NRR, as affirmed from surface-sensitive SERS detections of chemical species located near/at the bifunctional plasmonic and electrocatalytically active metallic surfaces (fig. S3). This direct molecular enrichment at the catalytic surface potentially enhances catalyst-gas collisions required for subsequent NRR without necessitating elevated temperature/pressure. The ZIF coating on the Ag-Au@ZIF electrode is also structurally robust upon thermal activation for the subsequent electrochemical NRR (fig. S2).

Electrochemical NRR investigations using the Ag-Au@ZIF electrode

We proceed to evaluate the performance of the Ag-Au@ZIF electrode for NRR at 298 K and 1 bar using a liquid-based electrochemical setup (Fig. 2A). The electrolyte system consists of "dry" tetrahydrofuran (THF)-solution containing lithium trifluoromethanesulfonate electrolyte and ~1 volume % ethanol as a biorenewable proton source for NRR. We use a three-electrode system comprising Pt wire as counter electrode and Ag/AgCl reference electrode to effect the electron-driven reactions at precisely controllable applied voltages.

To identify electroreduction of N_2 in our Ag-Au@ZIF electrode, we perform cyclic voltammetric investigations to elucidate the electrochemical processes occurring near the electrocatalytic surface. In the cathodic scan where the applied potential decreases from −0.5 to −3 V, Ag-Au@ZIF generates a distinct reduction peak at −2.5 V in the presence of N_2 bubbling [3 standard cubic centimeter per minute (sccm); Fig. 2B]. In the reverse anodic scan, we observe an electrochemical oxidation peak at ~−1.7 V as the voltage is regulated from −3 V back to the initial −0.5 V. In contrast, the reduction peak at −2.5 V is absent in a control setup under argon (Ar) bubbling [Fig. 2B (ii), brown trace]. We therefore eliminate the possibility that this reduction peak arises from electrochemical interference by ZIF, electrode material, or electrolyte solution. The clear difference in electrochemical responses upon exposure to different gases therefore affirms that the reduction peak at −2.5 V arises from N_2-related reduction processes.

On the other hand, the control Ag-Au electrode in the absence of ZIF coating exhibits two drastically different cathodic responses even though a similar anodic peak shows up at ~−1.6 V under identical test conditions (Fig. 2C). Specifically, the cyclic voltammogram recorded from the Ag-Au electrode under N_2 bubbling displays two new cathodic responses at −1.8 and −2.9 V in the forward scan, whereas the previously observed reduction peak at −2.5 V using Ag-Au@ZIF is not observed. Near-identical cyclic voltammetry features are also documented from the Ag-Au electrode when the bubbling gas is replaced from N_2 to Ar, evidently revealing that these two electrochemical peaks arise from electroactive species present in the electrolyte solution and are not N_2-related reactions. In addition, we exclude electroreduction of Ag cocatalyst as a possible cause of the cathodic peak at −2.5 V, because control HCl-treated Au electrode in the absence of Ag nanocubes also exhibits voltammogram akin to the Ag-Au platform (fig. S4A). From the differences in cathodic peaks in both Ag-Au@ZIF (at −2.5 V) and Ag-Au (at −1.8 and −2.9 V) platforms, it is clear that competing reducing species are present in the electrolyte solution, and these electrochemical interferences can be minimized by coating ZIF over the electrocatalyst. We then proceed to design comprehensive investigations to rationalize the electrochemical features from our Ag-Au@ZIF electrode and control Ag-Au platform without ZIF coating. We examine the distinct electrochemical features present in the voltammogram according to the following sequence: (i) the cathodic peak at −2.5 V in Ag-Au@ZIF linked to the presence of N_2 gas, (ii) the universal anodic peak at ~1.7 V, and (iii) two cathodic peaks that are present only in the Ag-Au electrode in the absence of ZIF.

Rationalizing the electrochemical features in cyclic voltammograms

First, we establish the origin of the cathodic peak at −2.5 V in Ag-Au@ZIF as the electroreduction of N_2 into ammonia. Briefly, we subject the Ag-Au@ZIF electrode to continuous N_2 flow for 6 hours at an applied potential of −2.9 V, which is slightly more negative than the peak potential of −2.5 V. The enhanced reducing capabilities at −2.9 V allow more rapid ammonia formation for accurate ammonia quantification by minimizing potential complications that could arise from solvent evaporation, especially in our open electrochemical system. We also

Downloaded from http://advances.sciencemag.org/ on August 19, 2018

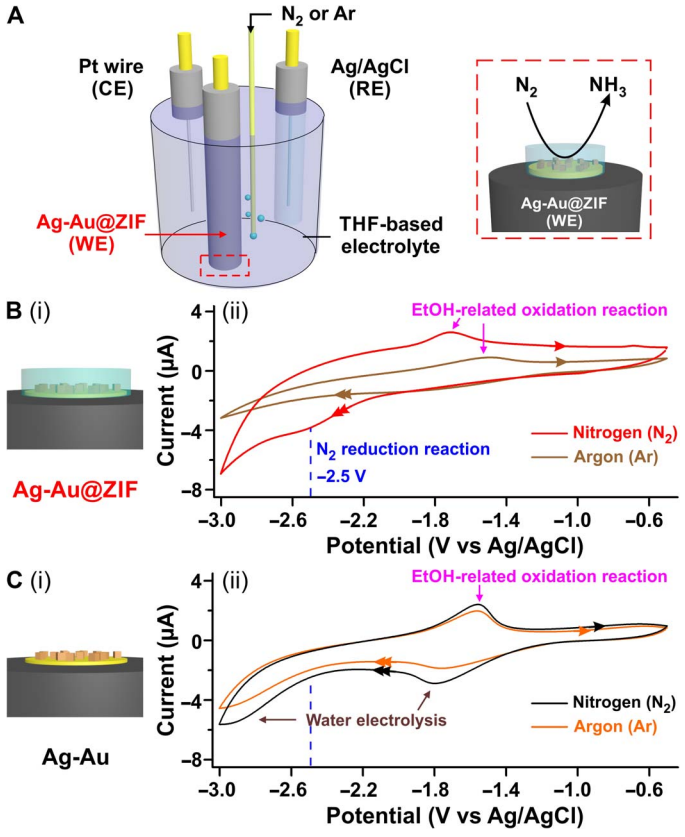

Fig. 2. Electrochemical reduction of N_2 gas using the Ag-Au@ZIF electrode. (**A**) Schematic illustrating the experimental setup of liquid electrolyte-based electrochemical reduction of N_2 gas to ammonia (inset). The electrolyte solution is prepared in dry tetrahydrofuran (THF). Various platforms prepared on Au electrodes function as the working electrode (WE). Pt wire and Ag/AgCl (1 M KCl) are used as counter (CE) and reference electrodes (RE), respectively. Cyclic voltammetry analysis using (**B**) Ag-Au@ZIF electrodes and (**C**) Ag-Au electrodes, both under argon (Ar) or N_2 gas bubbling. (i) Scheme depicting the respective working electrodes. (ii) Cyclic voltammograms recorded from respective working electrodes under Ar or N_2 gas bubbling. Directions of forward and backward scans are denoted by the double and single arrows, respectively. All gases are bubbled at 3 sccm using a mass flow controller.

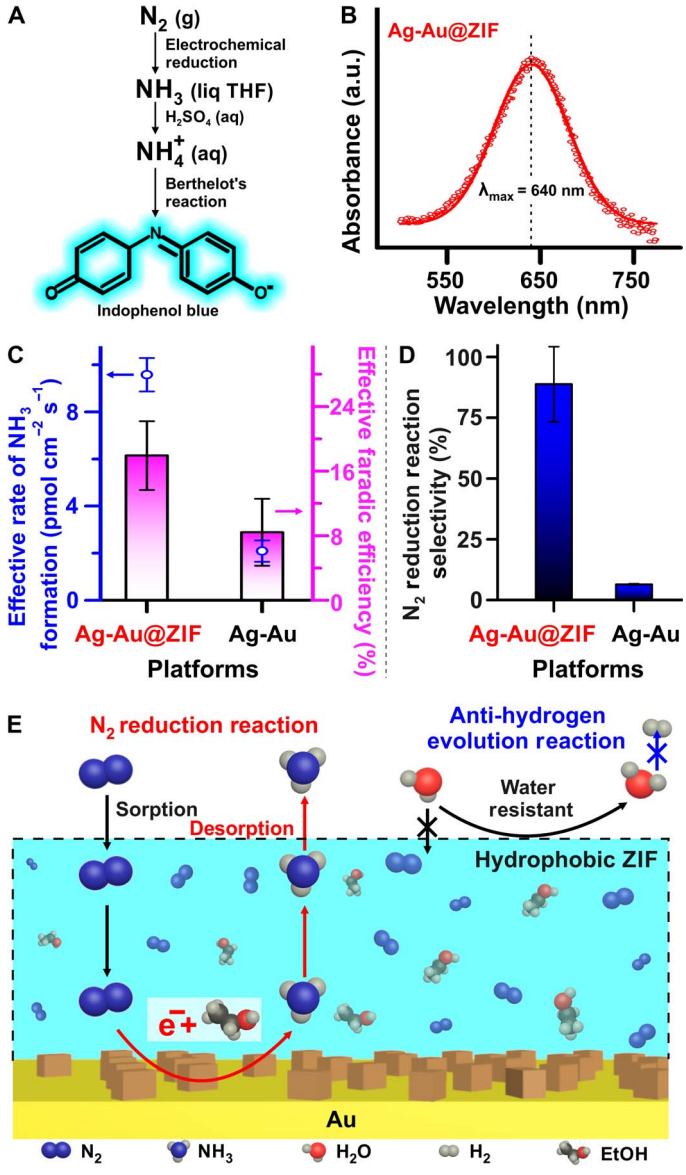

Fig. 3. Evaluation of electrochemical performance and selectivity toward NRR using Ag-Au@ZIF electrodes. (**A**) Experimental scheme for the electrochemical reduction of N_2 and subsequent quantification of the ammonia generated. Ammonia detection is based on the indophenol blue method. (**B**) Absorption spectra of indophenol blue formed from the ammonia generated using the Ag-Au@ZIF electrode under N_2 bubbling. (**C**) Effective rate of ammonia formation and Faradic efficiency for various electrode platforms. (**D**) Comparison of NRR selectivity in the presence and absence of ZIF encapsulation. (**E**) Overall process mechanism for the selective and improved electrochemical reduction of N_2 gas to form ammonia achieved simply by encapsulation with ZIF. ZIF layer functions both as a water-resistant coating and gas concentrator. N_2 is electrochemically reduced to generate ammonia (left). Water molecules are deterred from accessing the electroactive surface by a hydrophobic ZIF coating, hence impeding the competing HER (right).

adopt these electrochemical conditions in subsequent experiments involving other electrode platforms for a fairer comparison. Electrosynthesized ammonia is directly harvested from the THF-based electrolyte solution (ammonia solubility of ~0.4 M) by adding aqueous sulfuric acid to convert dissolved ammonia into ammonium ions. The amount of ammonia generated in the electrochemical process can thus be quantified from these ammonium ions using the indophenol blue method (Fig. 3A) (*28*). In this method, ammonium ions are converted back to ammonia in situ, which subsequently serves as a vital reagent in the Berthelot's reaction to generate indophenol blue. Ultraviolet-visible (UV-vis) spectroscopy measurement of the electrolyte solution after 6 hours of continuous N_2 flow exhibits an intense absorption peak at 638 nm that is characteristic of indophenol blue (Fig. 3B). This presence of NH_3 is concrete and unambiguous proof of ammonia formation via the electroreduction of N_2 in our Ag-Au@ZIF platform at −2.5 V. Our strategy of encapsulating electrocatalyst with MOF is therefore the first to enable direct electrochemical readout attributed to NRR at a remarkable experimental condition of 298 K and 1 bar, notably by mitigating the persistent electrochemical interferences arising from the favored water/moisture electrolysis (*13*). Identifying the electrochemical feature unique to NRR is critical to allow future thorough investigations on the thermodynamics and kinetics of electrochemical nitrogen-to-ammonia conversions to further optimize their efficiency and selectivity.

Downloaded from http://advances.sciencemag.org/ on August 19, 2018

To index the universal anodic peak at ~−1.7 V, we conduct cyclic voltammetry of Ag-Au@ZIF in the same electrolyte solution and under N_2 bubbling but without ethanol. We observe a featureless cyclic voltammogram without any anodic peak at −1.7 V (fig. S4B), hence highlighting its origin as an ethanol-related oxidation reaction. We further justify our assignment based on a similar lack of electrochemical response at ~−1.7 V, using the Ag-Au platform and water as the electrocatalyst and protic solvent, respectively (fig. S4C). Moreover, the absence of cathodic peak at −2.5 V even under N_2 bubbling clearly indicates that ethanol is required as a sole proton source for NRR.

Likewise, we unravel the two cathodic peaks unique to the Ag-Au electrode at −1.8 and −2.9 V as the consequence of water electrolysis by deliberately spiking the electrolyte solution with 20 volume % water. Under constant Ar bubbling, we detect an intense and linear current response in the reduction scan with magnitude in the mA regime (fig. S4D). This linear correlation in the water-spiked control solution begins at a potential of ~−1.3 V (fig. S4D, ii), corresponding well with the onset potential (~−1.2 V) of the first cathodic peak centered at −1.8 V when dry THF solution is used (Fig. 2C). It is also noteworthy that gas bubbles are rapidly evolved from the Ag-Au electrode in electrolyte solution spiked with water. Hence, the first and second cathodic peaks using bare Ag-Au electrode are likely due to the electrolysis of water present in the electrolyte solution, beginning with the HER (−1.8 V) and followed by hydride formation (−2.9 V) as the potential becomes more reductive (*29*).

The existence of HER despite the use of dry liquid THF highlights the detrimental effect that trace water content has on the electrochemical NRR system, which is unavoidable especially when water vapor is prevalent in the atmosphere. This creates an inevitable bottleneck to water-sensitive reactions and their electrochemical investigations, hence heavily restricting their practicability in applications beyond precisely controlled laboratory-based environments. Furthermore, the water-resistant properties conferred to electrocatalyst are possible only upon the complete overgrowth of ZIF over its surface; control Ag-Au electrode drop-casted with preformed ZIF nanoparticle exhibits dual cathodic peaks similar to the Ag-Au electrode without the ZIF encapsulation (fig. S4E). Collectively, our electrochemical findings highlight that vital reaction precursors can easily access the electrocatalyst surface, and also emphasize the importance of coating a hydrophobic ZIF layer over the electrocatalyst to perform water-sensitive reactions such as NRR; otherwise, the access of water to the catalyst will lead to overwhelming cathodic responses arising from HER.

Electrochemical performance of the Ag-Au@ZIF ensemble

We further determine the effective rate of ammonia formation (r_{NH3}) and Faradic efficiency to exemplify Ag-Au@ZIF as an efficient catalyst-MOF hybrid for the fixation of inert N_2 molecules into highly valuable ammonia. Rapid ammonia formation is essential to meet global demand, while high Faradic efficiency maximizes the utilization of electrons used to electrosynthesize ammonia. These effective values are obtained by comparing the measurement under N_2 bubbling against control Ar flow (*5*), hence enabling a more accurate assessment that eliminates background contributions due to remnant dissolved N_2, exposure to air, and/or nitrogen-containing species in chemical/solvent used. All ammonia harvesting experiments are performed by subjecting various electrode/gas combinations to a constant potential of −2.9 V over an accumulation period of 6 hours. For the Ag-Au@ZIF electrode, the average effective r_{NH3} is ~10 pmol cm^{-2} s^{-1} (Fig. 3C and figs. S5 and S6A), which is comparable to many previous reports where more catalytically active metals are used (*14*). We also affirm that the effective NH_3 molecules detected mainly originate from the nitrogen-to-ammonia conversion with negligible contribution from potential NH_3 contaminant in the input N_2 stream (~1%; fig. S6). Normalizing r_{NH3} with the current density (fig. S6), our Ag-Au@ZIF achieves a Faradic efficiency of 18 ± 4% for electrochemical nitrogen-to-ammonia conversion at ambient conditions (fig. S6B), surpassing conventional liquid-based electrochemical approach and solid-state electrochemistry operated at extreme pressure and temperature by >18-fold (*14*). Furthermore, our Ag-Au@ZIF electrode also achieves r_{NH3} and Faradic efficiency >4-fold and 2-fold superior to control Ag-Au platform in the absence of ZIF encapsulation, respectively. The latter suffers reduced performance due to competing electrolysis of water even at trace level in dry solution. We also note the relatively higher intrinsic efficiency of our liquid-based setup compared to other electrochemical approaches and attribute this to the use of dry organic liquid and presence of ionic electrolyte for efficient current flow. Nevertheless, our catalyst@MOF ensemble clearly offers a powerful approach to enhance reaction performance even at ambient conditions, whereby a boost to Faradic efficiency by 10 percentage point is attained simply by encapsulating electrocatalyst with a MOF layer. This achievement is notably significant considering the typical <1% Faradic efficiency reported for majority of previous NRR works (*14*, *15*). The Ag-Au@ZIF electrode also enables a >4-fold improvement to both turnover number and frequency (fig. S6, C and D), which are two common indicators used in catalysis studies to estimate the longevity and specific activity of a catalyst, respectively.

Notably, the ZIF coating in the Ag-Au@ZIF electrode also contributes to a high selectivity of ~90% toward NRR that is 14-fold better than the Ag-Au electrode in the absence of ZIF (Fig. 3D). This selectivity is derived from comparison of the Faradic currents obtained under N_2 and Ar flow to determine the percentage of current used for the entire NRR (fig. S7). The superior Faradic performance and selectivity to NRR in Ag-Au@ZIF arise from the efficient isolation and confinement of target trace reactants/additives on the catalyst's surfaces. This is possible because of the hydrophobic interior of nanoporous ZIF which is impermeable to trace water (≤1 volume %; fig. S8A), thus impeding HER which could otherwise consume the supplied electron and reduce the Faradic efficiency (Fig. 3E). Consequently, N_2 gas reactants infuse the ZIF scaffold selectively and eventually concentrate near the electrocatalyst surface driven by the thermodynamically favorable sorption at the interfacial cavities and ZIF's micropores (*18*). The close proximity of N_2 molecules and ethanol (proton source) to the catalytic surface facilitates both intermolecular and surface interactions, eventually activating the electrochemical heterogeneous reduction of N_2 molecules to ammonia when an external voltage is applied. Our Ag-Au@ZIF is also superior to the Au@ZIF platform comprising a single metal catalyst, where the latter exhibits a weak reducing peak at a more negative potential of −2.66 V (fig. S8B) and a correspondingly lower Faradic efficiency of 11 ± 2%. The need of a higher overpotential to drive NRR and poorer Faradic efficiency therefore indicates that it is more difficult for N_2 to be electrochemically reduced in a single metallic Au@ZIF platform. These observations therefore clearly exemplify the necessity of inherently stronger catalytic activities, either conferred by synergistic effect of bimetallic system or other NRR catalytic materials (*30*), to further promote reaction efficiency and offer distinct electrochemical responses for reaction studies. These findings also highlight that our electrocatalytic design is versatile and can be possibly build-on traditionally highly active Ru/Fe/Mo-based catalysts to confer NRR selectivity critical for overcoming their current performance bottleneck imposed by water poisoning (*13*).

Downloaded from http://advances.sciencemag.org/ on August 19, 2018

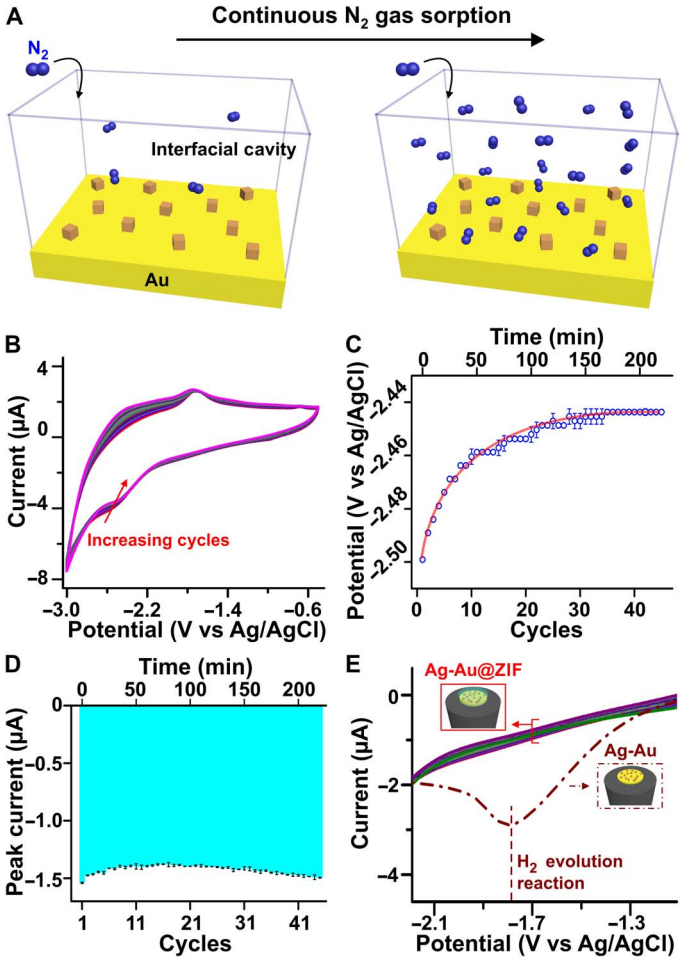

Fig. 4. Enhancing and sustaining electrochemical N_2 reduction performance using the Ag-Au@ZIF electrode. (**A**) Schematic depicting the continuous accumulation of N_2 molecules near the electrocatalyst to boost the performance of NRR. (**B**) Cyclic voltammograms depicting electrochemical responses indexed to NRR using Ag-Au@ZIF for 45 cycles. The red arrow denotes the systematic evolution of the electrochemical responses. (**C**) Peak potentials and (**D**) peak heights derived from the cyclic voltammograms in (B). (**E**) Magnified cyclic voltammograms near the HER region recorded from Ag-Au@ZIF electrodes for 45 cycles. A control voltammogram recorded from the Ag-Au electrode in the absence of ZIF encapsulation is included to indicate the potential region for HER. All experiments are performed under constant N_2 gas bubbling.

Enhanced and sustained NRR performance using the Ag-Au@ZIF platform

Time-dependent electrochemical evaluation of the Ag-Au@ZIF electrode also unveils enhanced electrochemical performance toward NRR via the molecular concentrating effect imparted by MOF (Fig. 4A). Continuous cyclic voltammetry examinations using the Ag-Au@ZIF electrode under constant N_2 bubbling demonstrate similar and distinct electrochemical features of NRR and ethanol-related oxidations at −2.5 and −1.7 V, respectively, throughout the 45 potential cycles (Fig. 4B). We note the concomitant positive shift of NRR peak potential from the initial −2.50 to ~−2.46 V at 50 min, eventually reaching a plateau of peak potential at −2.44 V beyond 170 min (Fig. 4C). Further resorption of N_2 and subsequent exposure of the Ag-Au@ZIF electrode to a second set of cyclic voltammetry treatment also yields similar peak potential of −2.44 V (fig. S9). It is noteworthy that the temporal positive shift of a reducing peak is a direct indication of the growing ease of N_2 electrochemical reduction. We attribute this phenomenon to the continuous sorption of reactants into a pseudo high-pressure microenvironment within the nanoscopic interfacial cavities (*18*), where reactants are forced near the electrocatalytic surface to improve reactants' accessibility and enhance catalyst-gas interaction necessary for NRR. Under sustained N_2 gas flow, this accumulation of reactants at the electrocatalyst surfaces ensures the abundance of N_2 molecules to fuel NRR, which is observed from the consistent peak current of 1.43 μA with <3% change over 45 consecutive cycles (Fig. 4D). The ZIF functionality in the Ag-Au@ZIF ensemble is also robust under extensive electrochemical treatment and able to retain its water-resistant properties throughout our experiments (Fig. 4E and fig. S9). Our results jointly demonstrate that MOF is essential to locally saturate and ensure an abundant supply of reactant molecules to the electrocatalytic surfaces, effectively overcoming the rapid depletion of chemical species near the catalytic sites in the absence of sorbing materials (fig. S10). This is especially crucial for electrocatalysis involving trace reactants/additives and/or sparsely distributed gaseous precursors that are prevalent in energy-related and electrosynthetic applications (*31*).

DISCUSSION

Our work highlights the importance of a superhydrophobic MOF coating on an electrocatalyst to favor the originally unfavored electrochemical NRR over competing water electrolysis, as well as impart a molecular concentrating effect to improve reactant-catalyst interactions. Using this reticular chemistry approach, we achieve both excellent selectivity toward NRR (~90%) and a boost to Faradic efficiency by 10 percentage points notably at ambient conditions. In comparison, many NRR studies report <1% Faradic efficiency at elevated temperature/pressure. Extensive electrochemical investigations unveil the unprecedented electrochemical response directly attributable to NRR, exemplifying the importance of hydrophobic MOF coating to suppress the competing HER and to accumulate N_2 molecules at catalyst surface for enhanced NRR. Our strategy effectively tackles the HER-induced bottleneck of NRR and allows future validation of theoretical models to accurately predict the thermodynamics of electrochemical nitrogen-to-ammonia conversion. Together with the build-on nature of our approach, which allows facile integration with intrinsically highly active catalytic materials, these valuable insights create enormous opportunities to design an ideal electrocatalytic system for high-performance and sustainable NRR even when using atmospheric air as feedstock. Our strategy could also be potentially extended to other electrochemical systems involving water-sensitive reactions.

MATERIALS AND METHODS

Chemicals

Silver nitrate (≥99%), anhydrous 1,5-pentanediol (PD; ≥97%), poly(vinylpyrrolidone) (PVP; average molecular weight, 55,000), zinc acetate dihydrate (≥98%, ACS reagent), 4,5-dichloroimidazole (≥98%), lithium trifluoromethanesulfonate ($LiCF_3SO_3$; 99.995%), sodium nitroprusside dihydrate (≥99%, ACS reagent; Reag. Ph. Eur), ammonium sulfate (≥99.0%), sodium dichloroisocyanurate dihydrate (≥98.0%), and phenol (≥99%, purified by redistillation) were purchased from Sigma-Aldrich. Copper (II) chloride (≥98%) was from Alfa Aesar. Methanol (≥99.9%) and THF (≥99.0%, ACS reagent) were from Fulltime. Ethanol (ACS, ISO, Reag. Ph Eur) and sodium hydroxide (NaOH;

Downloaded from http://advances.sciencemag.org/ on August 19, 2018

≥99.0%) were from EMSURE. *N*,*N*′-dimethylformamide (DMF; ACS reagent) was obtained from Tedia. Sulfuric acid (≥95%) and hydrochloric acid (37%) were from VWR Chemicals. Nitrogen (N_2; 99.999%, ALPHAGAZ 1) and argon (Ar; 99.9995%) were purchased from Singapore Oxygen Air Liquide Pte Ltd. THF was further dried by distilling commercial THF with sodium and benzophenone under inert N_2 environment. All other chemicals were applied without further purification. Milli-Q water (>18.0 megohm·cm) was purified with a Sartorius Arium 611 UV ultrapure water system.

Synthesis and purification of Ag nanocubes

The preparation of Ag nanocubes was carried out following the method described in the literature (*23*). Briefly, 10 ml of copper (II) chloride (8 mg/ml), PVP (20 mg/ml), and silver nitrate (20 mg/ml) were separately dissolved in PD. The chemicals were sonicated and vortexed repeatedly to dissolve them. Copper (II) chloride solution (35 μl) was then added to the silver nitrate solution. Then, 20 ml of 1,5-pentanediol in a 100-ml round bottomed flask was heated to 190°C for 10 min. PVP precursor (250 μl) was added to the flask dropwise every 30 s, whereas 500 μl of silver nitrate precursor was injected every minute using a quick addition. The addition process continued until the greenish coloration of the reaction mixture faded off.

For the purification of Ag nanocubes, PD was first removed from the mixture through centrifugation. The Ag nanocube solution was then dispersed in 10 ml of ethanol and 100 ml of aqueous PVP solution (0.2 g/liter). The resulting solution was vacuum-filtered using Durapore polyvinylidene fluoride filter membranes (Millipore) with pore sizes of 5000, 650, 450, and 220 nm, repeated several times for each pore size. The Ag nanocubes were later redispersed in ethanol. SEM imaging was performed, and the edge lengths of 100 Ag nanocubes were measured and analyzed using ImageJ software.

Preparation of the Ag-Au electrode

To prepare the Ag-Au electrode, 0.132 μl of ethanolic PVP-capped Ag nanocube solution was drop-casted onto a prepolished Au electrode (2-mm diameter). The electrode was then immersed in 0.1 M HCl solution (20% ethanol in water) for 3 hours and washed with a copious amount of methanol. The as-prepared Ag-Au electrode was dried using a stream of N_2 gas and stored under inert N_2 condition.

Encapsulation of the Ag-Au electrode with zeolitic imidazolate framework-71 (Ag-Au@ZIF electrode)

Before ZIF synthesis, methanolic solutions of zinc acetate dihydrate (0.2 M) and 4,5-dichloroimidazole (0.4 M) were prepared separately. As-prepared Ag-Au electrode was subsequently immersed into a 2-ml centrifuge tube containing 0.125 ml of DMF, 0.375 ml of MeOH, and 0.25 ml of respective methanolic solutions of zinc and imidazole precursors. The reaction was allowed for 40 min and later washed with a copious amount of methanol. ZIF formation reaction was repeated four more times to achieve a complete encapsulation over the Ag-Au surface. The electrode was dried using a stream of N_2 gas and stored under inert N_2 condition.

Preparation of the Au@ZIF electrode

Prepolished Au electrode was immersed in 0.1 M HCl solution (20% ethanol in water) for 3 hours and washed with a copious amount of methanol. The HCl-treated Au electrode was subsequently immersed into a 2-ml centrifuge tube containing 0.125 ml of DMF, 0.375 ml of MeOH, and 0.25 ml of respective methanolic solutions of zinc (0.2 M) and imidazole (0.4 M) precursors. The reaction was allowed for 40 min and later washed with a copious amount of methanol. ZIF formation reaction was repeated four more times to achieve a complete encapsulation over the Au surface. The electrode was dried using a stream of N_2 gas and stored under inert N_2 condition.

Encapsulating Ag nanocube drop-casted Au substrate with ZIF (Ag-Au@ZIF substrate)

Au films were first prepared using a thermal evaporator deposition system from Syskey Technology Corporation. An 18-nm Au was deposited on an O_2 plasma-treated Si wafer (0.6 cm × 0.6 cm) at a deposition rate of 0.8 Å/s. The deposited rate was monitored in situ by a quartz crystal microbalance. Au source with 99.99% purity was purchased from Zhongnuo Advanced Material (Beijing) Technology Co. Ltd.

Ethanolic solution of Ag nanocubes was drop-casted onto the Au substrate (Ag-Au substrate) at a volume-to-area ratio of ~4×10^{-2} μl/mm^2, which is also similar to that used for the Ag-Au and Ag-Au@ZIF electrodes. Upon drying, the Ag-Au substrate was subsequently immersed into a 2-ml centrifuge tube containing 0.125 ml of DMF, 0.375 ml of MeOH, and 0.25 ml of respective methanolic solutions of zinc (0.2 M) and imidazole (0.4 M) precursors. The reaction was allowed for 40 min and later washed with a copious amount of methanol. ZIF formation reaction was repeated four more times to achieve a complete encapsulation over the Ag-Au surface. The Ag-Au@ZIF substrate was dried using a stream of N_2 gas and stored under inert N_2 condition before subsequent cross-sectional SEM imaging and XRD characterizations.

Synthesis of ZIF nanoparticles

ZIF nanoparticles were synthesized from a reaction mixture containing 0.125 ml of DMF, 0.375 ml of MeOH, and 0.25 ml of respective methanolic solutions of zinc (0.2 M) and imidazole (0.4 M) precursors. The reaction was allowed for 40 min, washed with a copious amount of methanol, and subsequently redispersed in methanol.

Thermal activation of various platforms

Before latter application in electrochemical nitrogen-to-ammonia conversion, all platforms were thermally activated at 120°C under vacuum for 2 hours to evacuate residual methanol residing in ZIF's intrinsic pores after its synthesis. This heat treatment does not alter the structural and chemical identity of our platform, ensuring the integrity of its respective constituents for efficient and selective electrochemical reaction.

Electrochemical NRR

Electrolyte solutions were prepared by adding $LiCF_3SO_3$ (0.2 M) in a solvent mixture containing ~1% ethanol in dry THF. The THF-based electrolyte solutions were bubbled with respective N_2 or Ar gas for at least 15 min before electrochemical experiments. These gas flows were also maintained during the electrochemical measurements. All gas flow rates were controlled at ~3 sccm using mass flow controllers (model no. MC-100SCCM-D) obtained from Alicat Scientific Inc.

A three-electrode electrochemical setup was used, where the counter electrode and reference electrode were composed of a Pt wire and silver/silver chloride electrode (Ag/AgCl; 1 M KCl solution), respectively. Working electrodes were composed of thermal-activated Ag-Au@ZIF electrode as well as control platforms such as Ag-Au and Au@ZIF electrodes. Cyclic voltammetry measurements were recorded at a scan rate of 50 mV/s between applied potential of −3 and −0.5 V (versus Ag/AgCl).

Downloaded from http://advances.sciencemag.org/ on August 19, 2018

Electrolyte solutions and type of gas used were also varied to identify the electrochemical peaks recorded from different working electrodes. Electrochemical conversions of nitrogen to ammonia for evaluation of Faradic efficiency and ammonia formation rate were subsequently conducted using chronoamperometry at a constant applied potential of −2.9 V for 6 hours using respective combinations of working electrode and gas types. Ammonia generated was quantified using the indophenol blue method (stated in the following sections). All electrochemical experiments were performed under constant gas flow and at ambient conditions of 1 bar and 298 K.

Preparation of reagents for indophenol blue method

Two precursor solutions were required in the indophenol blue method and were named as reagent A and reagent B, respectively (*28*). Reagent A was prepared by dissolving phenol (0.1 M) and sodium nitroprusside dihydrate (0.2 mM) in water. Reagent B was prepared by dissolving sodium dichloroisocyanurate dihydrate (2.8 mM) and NaOH (0.13 M) in water. Both reagents were stored in the fridge before use.

Detection of ammonia using indophenol blue method

A calibration curve relating extinction intensity with ammonia/ammonium concentration was first established for subsequent quantification of ammonia produced in the electrochemical reaction. Ammonium sulfate (10 mM) was dissolved in an aqueous sulfuric acid solution (10^{-3} M). The ammonium sulfate was then serial-diluted to various concentrations between 10^{-6} and 10^{-4} M. After which, an equivalent amount of dry THF (containing 1% ethanol) was added to all the ammonium sulfate standard solutions. Individual ammonium sulfate standard solution (0.2 ml) was added to a glass vial containing 1 ml of reagent A. One milliliter of reagent B was then added into the solution and allowed to react for 1 hour while being stirred at 500 rpm. Indophenol blue generated was identified and quantified using UV-vis spectroscopy (*28*).

To determine the ammonia generated during the electrochemical nitrogen-to-ammonia conversion, we added the THF-based electrolyte solution to an equivalent amount of aqueous sulfuric acid solution (10^{-3} M). Two milliliters of this solution was added to a glass vial containing 1 ml of reagent A. One milliliter of reagent B was then added into the solution and allowed to react for 1 hour while being stirred at 500 rpm. Indophenol blue generated was identified and quantified using UV-vis spectroscopy. THF electrolyte solutions were primarily examined for ammonia because THF readily dissolves ammonia up to a high concentration of 0.4 M.

Determination of rate of ammonia formation and Faradic efficiency

The ammonia formation rate and Faradic efficiency were calculated using Eqs. 1 and 2, respectively (*32*)

$$r_{NH_3} = \frac{[NH_4^+] \times V}{t \times A} \quad (1)$$

where r_{NH3} is the rate of ammonia formation (mol cm^{-2} s^{-1}), $[NH_4^+]$ is the concentration of produced ammonium ion (equivalent to ammonia concentration), V is the volume of THF-based electrolyte solution, t is time of collection, and A is the overall electrocatalyst's area.

$$\text{Faradic efficiency } (\%) = \frac{3F \times r_{NH_3}}{I} \quad (2)$$

where r_{NH3} is the rate of ammonia formation, I is the current density at constant applied voltage, and F is the Faraday constant.

SERS evaluation

The thermal-activated electrodes and the electrolyte solution were placed inside a custom-made gas flow cell with a quartz window suitable for SERS examination. N_2 gas was bubbled in the electrolyte solution for at least 15 min before SERS measurement and maintained during entire experiments. N_2 gas flow was precisely controlled at 3 sccm. All SERS spectra were normalized between 0 (min) and 1 (max).

Material characterization

SEM and energy-dispersive x-ray spectroscopy imaging were performed with JEOL-JSM-7600F microscope. UV-vis spectroscopic measurements were conducted with a Cary 60 UV-vis spectrometer. SERS measurements were performed using *x-y* hyperspectral imaging mode of the Ramantouch microspectrometer (Nanophoton Inc.) with an excitation wavelength of 532 nm. Using a 50× (numerical aperture, 0.45) objective lens, the laser power was preset at 0.37 mW with 5-s accumulation time for data collection between 200 and 2600 cm^{-1}. All SERS spectra were the average of at least nine individual spectrum. Substrate XRD patterns were recorded on a Bruker General Area Detector Diffraction System (GADDS) XRD diffractometer with Cu Ka radiation. All electrochemical experiments were performed using Metrohm Autolab potentiostat instrument.

SUPPLEMENTARY MATERIALS

Supplementary material for this article is available at http://advances.sciencemag.org/cgi/content/full/4/3/eaar3208/DC1

fig. S1. Characterization of as-synthesized and HCl-treated Ag nanocubes.
fig. S2. Characterization of the Ag-Au@ZIF platform.
fig. S3. Qualitative comparisons of SERS spectra obtained under various experimental conditions.
fig. S4. Electrochemical investigations of various electrodes under respective conditions.
fig. S5. Calibration of the indophenol blue method for subsequent NH_3/NH_4^+ quantification.
fig. S6. Evaluating the performance of the Ag-Au@ZIF ensemble over control platforms.
fig. S7. Selectivity of various electrode platforms toward NRR.
fig. S8. Water-repelling properties of Ag-Au@ZIF and cyclic voltammetry analysis on Au@ZIF.
fig. S9. Enhancing and sustaining electrochemical N_2 reduction performance using the Ag-Au@ZIF electrode.
fig. S10. Time-dependent electrochemical evaluation of the Ag-Au electrode.
References (*33*–*37*)

REFERENCES AND NOTES

1. J. W. Erisman, M. A. Sutton, J. Galloway, Z. Klimont, W. Winiwarter, How a century of ammonia synthesis changed the world. *Nat. Geosci.* **1**, 636–639 (2008).
2. R. F. Service, New recipe produces ammonia from air, water, and sunlight. *Science* **345**, 610 (2014).
3. C. J. M. van der Ham, M. T. M. Koper, D. G. H. Hetterscheid, Challenges in reduction of dinitrogen by proton and electron transfer. *Chem. Soc. Rev.* **43**, 5183–5191 (2014).
4. C. Liu, K. K. Sakimoto, B. C. Colón, P. A. Silver, D. G. Nocera, Ambient nitrogen reduction cycle using a hybrid inorganic–biological system. *Proc. Natl. Acad. Sci. U.S.A.* **114**, 6450–6455 (2017).
5. K. A. Brown, D. F. Harris, M. B. Wilker, A. Rasmussen, N. Khadka, H. Hamby, S. Keable, G. Dukovic, J. W. Peters, L. C. Seefeldt, P. W. King, Light-driven dinitrogen reduction catalyzed by a CdS:nitrogenase MoFe protein biohybrid. *Science* **352**, 448–450 (2016).
6. M. Ali, F. Zhou, K. Chen, C. Kotzur, C. Xiao, L. Bourgeois, X. Zhang, D. R. MacFarlane, Nanostructured photoelectrochemical solar cell for nitrogen reduction using plasmon-enhanced black silicon. *Nat. Commun.* **7**, 11335 (2016).
7. J. Rittle, J. C. Peters, An Fe-N_2 complex that generates hydrazine and ammonia via Fe=NNH_2: Demonstrating a hybrid distal-to-alternating pathway for N_2 reduction. *J. Am. Chem. Soc.* **138**, 4243–4248 (2016).
8. T. Oshikiri, K. Ueno, H. Misawa, Selective dinitrogen conversion to ammonia using water and visible light through plasmon-induced charge separation. *Angew. Chem. Int. Ed.* **55**, 3942–3946 (2016).

Downloaded from http://advances.sciencemag.org/ on August 19, 2018

9. S. Licht, B. Cui, B. Wang, F.-F. Li, J. Lau, S. Liu, Ammonia synthesis by N_2 and steam electrolysis in molten hydroxide suspensions of nanoscale Fe_2O_3. *Science* **345**, 637–640 (2014).
10. G.-F. Chen, X. Cao, S. Wu, X. Zeng, L.-X. Ding, M. Zhu, H. Wang, Ammonia electrosynthesis with high selectivity under ambient conditions via a Li^+ incorporation strategy. *J. Am. Chem. Soc.* **139**, 9771–9774 (2017).
11. D. Bao, Q. Zhang, F.-L. Meng, H.-X. Zhong, M.-M. Shi, Y. Zhang, J.-M. Yan, Q. Jiang, X.-B. Zhang, Electrochemical reduction of N_2 under ambient conditions for artificial N_2 fixation and renewable energy storage using N_2/NH_3 cycle. *Adv. Mater.* **29**, 1604799 (2017).
12. A. R. Singh, B. A. Rohr, J. A. Schwalbe, M. Cargnello, K. Chan, T. F. Jaramillo, I. Chorkendorff, J. K. Nørskov, Electrochemical ammonia synthesis—The selectivity challenge. *ACS Catal.* **7**, 706–709 (2017).
13. J. N. Renner, L. F. Greenlee, K. E. Ayres, A. M. Herring, Electrochemical synthesis of ammonia: A low pressure, low temperature approach. *Electrochem. Soc. Interface* **24**, 51–57 (2015).
14. V. Kyriakou, I. Garagounis, E. Vasileiou, A. Vourros, M. Stoukides, Progress in the electrochemical synthesis of ammonia. *Catal. Today* **286**, 2–13 (2017).
15. S. Chen, S. Perathoner, C. Ampelli, C. Mebrahtu, D. Su, G. Centi, Electrocatalytic synthesis of ammonia at room temperature and atmospheric pressure from water and nitrogen on a carbon-nanotube-based electrocatalyst. *Angew. Chem. Int. Ed.* **56**, 2699–2703 (2017).
16. J. H. Montoya, C. Tsai, A. Vojvodic, J. K. Nørskov, The challenge of electrochemical ammonia synthesis: A new perspective on the role of nitrogen scaling relations. *ChemSusChem* **8**, 2180–2186 (2015).
17. J. G. Howalt, T. Bligaard, J. Rossmeisl, T. Vegge, DFT based study of transition metal nano-clusters for electrochemical NH_3 production. *Phys. Chem. Chem. Phys.* **15**, 7785–7795 (2013).
18. H. K. Lee, Y. H. Lee, J. V. Morabito, Y. Liu, C. S. L. Koh, I. Y. Phang, S. Pedireddy, X. Han, L.-Y. Chou, C.-K. Tsung, X. Y. Ling, Driving CO_2 to a quasi-condensed phase at the interface between a nanoparticle surface and a metal–organic framework at 1 bar and 298 K. *J. Am. Chem. Soc.* **139**, 11513–11518 (2017).
19. M. Tu, C. Wiktor, C. Rösler, R. A. Fischer, Rapid room temperature syntheses of zeolitic-imidazolate framework (ZIF) nanocrystals. *Chem. Commun.* **50**, 13258–13260 (2014).
20. R. P. Lively, M. E. Dose, J. A. Thompson, B. A. McCool, R. R. Chance, W. J. Koros, Ethanol and water adsorption in methanol-derived ZIF-71. *Chem. Commun.* **47**, 8667–8669 (2011).
21. Q.-L. Zhu, Q. Xu, Immobilization of ultrafine metal nanoparticles to high-surface-area materials and their catalytic applications. *Chem.* **1**, 220–245 (2016).
22. Q.-L. Zhu, J. Li, Q. Xu, Immobilizing metal nanoparticles to metal–organic frameworks with size and location control for optimizing catalytic performance. *J. Am. Chem. Soc.* **135**, 10210–10213 (2013).
23. H. K. Lee, Y. H. Lee, I. Y. Phang, J. Wei, Y.-E. Miao, T. Liu, X. Y. Ling, Plasmonic liquid marbles: A miniature substrate-less SERS platform for quantitative and multiplex ultratrace molecular detection. *Angew. Chem. Int. Ed.* **53**, 5154–5158 (2014).
24. S. Liu, G. Liu, X. Zhao, W. Jin, Hydrophobic-ZIF-71 filled PEBA mixed matrix membranes for recovery of biobutanol via pervaporation. *J. Membr. Sci.* **446**, 181–188 (2013).
25. S. Calero, P. Gómez-Álvarez, Underlying adsorption mechanisms of water in hydrophobic and hydrophilic zeolite imidazolate frameworks: ZIF-71 and ZIF-90. *J. Phys. Chem. C* **119**, 23774–23780 (2015).
26. Y. Li, L. H. Wee, J. A. Martens, I. F. J. Vankelecom, ZIF-71 as a potential filler to prepare pervaporation membranes for bio-alcohol recovery. *J. Mater. Chem. A* **2**, 10034–10040 (2014).
27. A. A. Talin, A. Centrone, A. C. Ford, M. E. Foster, V. Stavila, P. Haney, R. A. Kinney, V. Szalai, F. El Gabaly, H. P. Yoon, F. Léonard, M. D. Allendorf, Tunable electrical conductivity in metal-organic framework thin-film devices. *Science* **343**, 66–69 (2014).
28. A. Tsuneto, A. Kudo, T. Sakata, Lithium-mediated electrochemical reduction of high pressure N_2 to NH_3. *J. Electroanal. Chem.* **367**, 183–188 (1994).
29. A. J. Bard, R. Parsons, J. Jordan, *Standard Potentials in Aqueous Solution* (Taylor & Francis, 1985).
30. J. Lin, L. Zhang, Z. Wang, J. Ni, R. Wang, K. Wei, The effect of Ag as a promoter for Ru/CeO_2 catalysts in ammonia synthesis. *J. Mol. Catal. A Chem.* **366**, 375–379 (2013).
31. A. Q. Fenwick, J. M. Gregoire, O. R. Luca, Electrocatalytic reduction of nitrogen and carbon dioxide to chemical fuels: Challenges and opportunities for a solar fuel device. *J. Photochem. Photobiol. B* **152**, 47–57 (2015).
32. D. S. Yun, J. H. Joo, J. H. Yu, H. C. Yoon, J.-N. Kim, C.-Y. Yoo, Electrochemical ammonia synthesis from steam and nitrogen using proton conducting yttrium doped barium zirconate electrolyte with silver, platinum, and lanthanum strontium cobalt ferrite electrocatalyst. *J. Power Sources* **284**, 245–251 (2015).
33. L. He, Y. Liu, J. Liu, Y. Xiong, J. Zheng, Y. Liu, Z. Tang, Core–shell noble-metal@metal-organic-framework nanoparticles with highly selective sensing property. *Angew. Chem. Int. Ed.* **52**, 3741–3745 (2013).
34. D. Singh, Y. Li, S. C. Sharma, Effect of pressure on the Raman spectra of methanol–ethanol–water mixture at room temperature. *J. Raman Spectrosc.* **36**, 24–27 (2005).
35. J. Kiefer, F. Toni, K.-E. Wirth, Influence of carbon-coated iron nanoparticles on the Raman spectrum of liquid ethanol. *J. Raman Spectrosc.* **46**, 1124–1128 (2015).
36. F. Zhou, L. M. Azofra, M. Ali, M. Kar, A. N. Simonov, C. McDonnell-Worth, C. Sun, X. Zhang, D. R. MacFarlane, Electro-synthesis of ammonia from nitrogen at ambient temperature and pressure in ionic liquids. *Energy Environ. Sci.* **10**, 2516–2520 (2017).
37. A. Nalaparaju, X. S. Zhao, J. W. Jiang, Molecular understanding for the adsorption of water and alcohols in hydrophilic and hydrophobic zeolitic metal–organic frameworks. *J. Phys. Chem. C* **114**, 11542–11550 (2010).

Acknowledgments

Funding: X.Y.L. thanks the financial support from Singapore Ministry of Education Tier 1 (RG21/16) and Tier 2 (MOE2016-T2-1-043) grants. H.K.L. appreciates the Agency for Science, Technology and Research (A*STAR) Graduate Scholarship support from A*STAR, Singapore. C.S.L.K. acknowledges support from Nanyang Presidential Graduate Scholarship from Nanyang Technological University. C.L. was supported by Lee Kuan Yew Postdoctoral Fellowship, Singapore. C.-K.T. acknowledges support from Boston College and donors of the American Chemical Society Petroleum Research Fund. **Author contributions:** H.K.L. and X.Y.L. conceived and designed the research. H.K.L., C.S.L.K., I.Y.P., and X.H. performed the research. H.K.L., C.S.L.K., Y.H.L., C.L., C.-K.T., and X.Y.L. analyzed the results and wrote the manuscript. X.Y.L. supervised the project. All authors discussed and commented on the manuscript. **Competing interests:** The authors declare that they have no competing interests. **Data and materials availability:** All data needed to evaluate the conclusions in the paper are present in the paper and/or the Supplementary Materials. Additional data related to this paper may be requested from the authors.

Submitted 25 October 2017
Accepted 2 February 2018
Published 9 March 2018
10.1126/sciadv.aar3208

Citation: H. K. Lee, C. S. L. Koh, Y. H. Lee, C. Liu, I. Y. Phang, X. Han, C.-K. Tsung, X. Y. Ling, Favoring the unfavored: Selective electrochemical nitrogen fixation using a reticular chemistry approach. *Sci. Adv.* **4**, eaar3208 (2018).

Downloaded from http://advances.sciencemag.org/ on August 19, 2018

Science Advances

Favoring the unfavored: Selective electrochemical nitrogen fixation using a reticular chemistry approach

Hiang Kwee Lee, Charlynn Sher Lin Koh, Yih Hong Lee, Chong Liu, In Yee Phang, Xuemei Han, Chia-Kuang Tsung and Xing Yi Ling

Sci Adv **4** (3), eaar3208.
DOI: 10.1126/sciadv.aar3208

ARTICLE TOOLS http://advances.sciencemag.org/content/4/3/eaar3208

SUPPLEMENTARY MATERIALS http://advances.sciencemag.org/content/suppl/2018/03/05/4.3.eaar3208.DC1

REFERENCES This article cites 36 articles, 6 of which you can access for free
http://advances.sciencemag.org/content/4/3/eaar3208#BIBL

PERMISSIONS http://www.sciencemag.org/help/reprints-and-permissions

Use of this article is subject to the Terms of Service

Science Advances (ISSN 2375-2548) is published by the American Association for the Advancement of Science, 1200 New York Avenue NW, Washington, DC 20005. 2017 © The Authors, some rights reserved; exclusive licensee American Association for the Advancement of Science. No claim to original U.S. Government Works. The title *Science Advances* is a registered trademark of AAAS.

Downloaded from http://advances.sciencemag.org/ on August 19, 2018